



Available online at www.sciencedirect.com

ScienceDirect

Geochimica et Cosmochimica Acta 147 (2014) 90-106

Geochimica et Cosmochimica Acta

www.elsevier.com/locate/gca

Resolving the gap between laboratory and field rates of feldspar weathering

Chen Gruber a,*, Chen Zhu b, R. Bastian Georg c, Yevgeny Zakon d, Jiwchar Ganor a

a Department of Geological and Environmental Sciences, Ben-Gurion University of the Negev, P. O. Box 653, Beer-Sheva 84105, Israel
 b Department of Geological Sciences, Indiana University, Bloomington, IN 47405, USA

^c Water Quality Centre, Trent University, Peterborough, ON, Canada ^d Geological Survey of Israel, 30 Malkhe Israel, Jerusalem 95501, Israel

Received 26 June 2014; accepted in revised form 15 October 2014; available online 23 October 2014

Abstract

Weathering rates of silicate minerals observed in the laboratory are in general up to five orders of magnitude higher than those inferred from field studies. The differences between experimental conditions in the laboratory and natural conditions in the field have been thoroughly discussed in previous studies, however, the discrepancy was never fully resolved. It has been shown in past work that if the field conditions are fully simulated in standard laboratory experiments, it is not possible to measure the slow rates of mineral dissolution that are observed in the field using standard laboratory experiments. Therefore, a novel method that uses the change of Si isotopes ratio in spiked solutions is used in the present study to measure weathering rates of feldspar under close-to-natural conditions.

A single-point batch experiment (SPBE) of albite dissolution was performed in the present study with an "untreated" albite sample. During the SPBE the dissolution rate was affected by the change of deviation from equilibrium and by the change in the mineral surface reactivity. In order to quantify the effect of the change in surface reactivity on the measured dissolution rates, two multi-point batch experiments (MPBE) were conducted. In those experiments, surface reactivity was found to depend on the amount of dissolved mineral. The decrease in surface reactivity as a function of the amount of dissolved mineral may be described using empirical power laws.

Another MPBE was used to measure far-from-equilibrium dissolution rate of albite using a sample that lost most of the highly reactive sites and highly reactive fine crystal during the initial stage of the experiment. Therefore, the change of its surface reactivity is small over the duration of the laboratory experiment (henceforth, "treated" albite sample). Another SPBE was conducted to quantify the effect of deviation from equilibrium on albite dissolution rate under close-to-equilibrium using the "treated" albite sample.

For the first time, albite dissolution rate (or any silicate mineral) is described as a function of deviation from equilibrium under ambient temperature and circum neutral pH. Even though the new experimental results confirm the extrapolation of high temperature data, the measured dissolution rates were higher than those from field studies. Introducing a reactivity coefficient allows for resolving the discrepancy between dissolution rates observed in natural settings as opposed to experimental setups.

Our results indicate that the extensive debate on the gap between dissolution rates determined using laboratory experiments and those using field observations reflects the inability to measure the dissolution rates under typical field conditions, using standard laboratory experiments.

© 2014 Elsevier Ltd. All rights reserved.

E-mail address: chengrub@post.bgu.ac.il (C. Gruber).

^{*} Corresponding author. Tel.: +972 8 6477 517; fax: +972 8 6472

1. INTRODUCTION

Quantification and understanding of mineral weathering have important implications for many environmental problems, such as the relationship between silicate weathering and global climate over geological timescales (Berner, 1992), the availability of inorganic nutrients in soils (Federer et al., 1989; Likens et al., 1998; Huntington et al., 2000), geological carbon sequestration (White et al., 2003), global geochemical cycles (Lasaga et al., 1994), safety of radioactive waste repositories (Spycher et al., 2003), impacts of acid mines drainage and neutralization of acid precipitation in watersheds (Drever and Clow, 1995), release of toxic elements to soils and to the hydrologic cycle, and the distribution of porosity and permeability in hydrocarbon reservoir rocks (Morad et al., 2010). Weathering rates of silicate minerals observed in the laboratory are in general up to five orders of magnitude higher than those inferred from field studies (Schnoor, 1990; Stumm, 1992; van Grinsven and van Riemsdijk, 1992; Anbeek, 1993; Casey et al., 1993; Velbel, 1993; Blum and Stillings, 1995; White and Brantley, 1995, 2003; White et al., 1996, 2005, 2008; Drever, 2003; Zhu et al., 2004; Zhu, 2005; Ganor et al., 2007; Moore et al., 2012). The many differences between experimental conditions in the laboratory and natural conditions in the field have been thoroughly discussed in previous studies (e.g., White and Brantley, 2003; Reeves and Rothman, 2013, and references therein), but the discrepancy was never fully reconciled.

In short, it was suggested that the differences between laboratory and field rates result from: (i) efficiency of solution/mineral contact, (ii) duration of weathering, aging of surfaces, (iii) presence and depth of defects and etch pits, (iv) formation of leached layers, (v) surface coatings, (vi) degree of undersaturation, and solution chemistry in micro-pores. In contrast to natural weathering, laboratory experiments are usually conducted under conditions in which precipitation of secondary phases does not occur. If the field conditions are fully simulated in standard laboratory experiments, it is not possible to measure the slow rates of mineral dissolution that are observed in the field using standard laboratory experiments (Ganor et al., 2007). In the absence of laboratory data, geochemical modeling may be used to predict the change with time in reactants and products of chemical reactions (Zhu and Anderson, 2002). Geochemical models use rate laws that are based on experimental data but are extrapolated to time scales and conditions that were not tested experimentally. As these models deal with open systems, they cannot be verified (Oreskes et al., 1994); they may only be confirmed under conditions and time scales that typically apply to laboratory experiments.

In order to resolve the gap between laboratory measurements and field estimates of dissolution rates, a novel method that uses Si isotopes (Gruber et al., 2013) is used in the present study to measure weathering rates of feldspar under close-to-natural conditions. The results confirm the extrapolation of high temperature data and fully resolved

the gap between laboratory measurements and field estimates.

1.1. Rate dependency on deviation from equilibrium

Many studies on dissolution kinetics of feldspars, the most common silicates minerals in earth's crust, were conducted under conditions (i.e., temperature, pH, and deviation from equilibrium) in which dissolution is relatively fast (Knauss and Wolery, 1986; Casey et al., 1989, 1993; Lasaga, 1990; Burch et al., 1993; Blum and Stillings, 1995; Alekseyev et al., 1997; Chen and Brantley, 1997; Hellmann and Tisserand, 2006). The effect of each environmental variable, derived from such studies, is typically described using a simple rate law. For example, the dependence of the rate of an elementary reaction on the deviation from equilibrium is described based on the principle of detailed balancing or from Transition State Theory (TST) using the rate law (Rimstidt and Barnes, 1980; Helgeson et al., 1984; Lasaga, 1998):

$$Rate_{diss} = k \left(1 - \exp\left(\frac{\Delta G_r}{RT}\right) \right) \tag{1}$$

where k is a rate coefficient (mol m⁻² s⁻¹), ΔG_r is Gibbs free energy of the reaction (kJ mol⁻¹), R is the gas constant and T is the temperature in Kelvin. The dependence of the rate of an overall reaction, such as dissolution, is difficult to predict a priori. In many studies Eq. (1) is generalized to:

$$f(\Delta G_r) = 1 - \exp\left(\frac{n \cdot \Delta G_r}{RT}\right) \tag{2}$$

where n is a coefficient that is not necessarily equal to one (Lasaga, 1998). The form of Eq. (2) can be applied to overall reactions in a few simple cases that are described by Lasaga (1998). In all these cases, defects such as dislocations should not control the dissolution kinetics.

Eqs. (1) and (2) describe the effect of deviation from equilibrium on dissolution rate under conditions in which a single mechanism is dominant throughout the entire range of ΔG_r . However, there is a major change in the dominant reaction mechanism between the near-equilibrium and the far-from-equilibrium regions. This change in mechanism was attributed to the opening of etch pits once the solution is sufficiently undersaturated (Lasaga and Blum, 1986; Burch et al., 1993; Beig and Luttge, 2006).

In the present study the term "far-from-equilibrium" is used to describe conditions in which dissolution of the etch pits is the dominant mechanism and the rate is independent of the degree of saturation. This region in Rate vs. ΔGr space is termed the dissolution plateau (Lasaga et al., 1994). The term "near-to-equilibrium" is used to describe conditions under which the free energy is not sufficient for the opening of etch pits and dissolution occurs only on the bulk mineral surface and not on defects. The term "closer-to-equilibrium" is used to describe experiments that were conducted under the conditions of the transition between the two dissolution mechanisms.

In order to describe the effect of deviation from equilibrium on dissolution rates, the rate law should include the contribution of the dissolution of both the etch pits and the bulk mineral surface. Assuming that dissolution at these two sites is independent of each other, the overall dissolution rate will be the sum of the rates of the two mechanisms.

The effect of deviation from equilibrium on albite dissolution rate was studied by Burch et al. (1993) at 80 °C, pH 8.8 using a freshly ground Amelia albite and was described using the equation:

Rate_{diss} =
$$-k'_1 \left[1 - e^{8.4 \cdot 10^{-17} \cdot \left(\frac{\Delta G_r}{RT} \right)^{15}} \right] - k'_2 \left[1 - e^{\left(\frac{\Delta G_r}{RT} \right)} \right]^{1.45}$$
 (3)

where k'_1 and k'_2 are rate coefficients that depend on the environmental conditions. In contrast to the rate law of Eq. (1), this rate law is an empirical rate law, which is not based on kinetic theory.

Based on defect-generated dissolution stepwaves model, Lasaga and Luttge (2001) proposed a theoretical formulation that describes the variation of dissolution rate with the degree of undersaturation:

$$\operatorname{Rate}_{\operatorname{diss}} = k_1 (1 - e^{\Delta G_r / RT}) \tanh \left[\frac{B}{\left(1 - \frac{1 - e^{\frac{\Delta G_{\operatorname{crit}}}{RT}}}{1 - \frac{1 - e^{\frac{\Delta G_r}{RT}}}{RT}} \right)} \right] \left(1 - \frac{1 - e^{\frac{\Delta G_{\operatorname{crit}}}{RT}}}{1 - e^{\frac{\Delta G_r}{RT}}} \right)$$
(4

where k_1 is a rate constant (mol m⁻² s⁻¹), ΔG_{crit} is the Gibbs free energy that is required to form etch pits (kJ mol⁻¹), and B is a constant that depends on surface diffusion distance.

Eq. (4) described the dissolution at etch pits. This mechanism is the main contributor to dissolution under "far-from-equilibrium" conditions. Under "near-to-equilibrium" conditions, i.e., below the $\Delta G_{\rm crit}$ (the energy barrier that required to open an etch pits (Lasaga and Blum, 1986)), dissolution occurs only on the bulk mineral surface and not on defects and therefore may be described by TST (Eq. (1)). The overall dissolution rate law may be described as the sum of Eqs. (1) and (4):

$$\begin{aligned} \text{Rate}_{\text{diss}} &= k_1 (1 - e^{\Delta G_r / RT}) \text{tanh} \left[\frac{B}{\left(1 - \frac{1 - e^{\frac{\Delta G_{\text{crit}}}{RT}}}{\frac{\Delta G_r}{1 - e^{\frac{RT}{RT}}}} \right)} \right] \left(1 - \frac{1 - e^{\frac{\Delta G_{\text{crit}}}{RT}}}{1 - e^{\frac{\Delta G_r}{RT}}} \right) \\ &+ k_2 (1 - e^{\Delta G_r / RT}) \end{aligned} \tag{5}$$

Eq. (5) is based on the assumption that the overall dissolution rate is a sum of the two mechanisms of Eqs. (1) and (4). This assumption is discussed below in Section 4.1. The rate law of Eq. (5) predicts albite dissolution rates at various elevated temperatures (80 (Burch et al., 1993), 150 (Hellmann and Tisserand, 2006) and 300 °C (Alekseyev et al., 1997)) as is demonstrated in Fig. 1.

The rate law of Eq. (5) that describes the effect of deviation from equilibrium may be combined with rate laws that describe other effects (e.g., temperature) to a general rate law that describes the dependence of the reaction rate on the environmental conditions as a product of terms, assuming that they are independent of each other (Lasaga, 1995, 1998), e.g., assuming that the effect of deviation from equilibrium on reaction rate of Eq. (5) is temperature independent. The obtained general rate law may be used to predict the rate under conditions in which the rate cannot be experimentally determined using standard methods (Ganor et al., 2007).

1.2. Determination of dissolution rates

The change in concentration of the dissolved mineral's products in a batch reactor may be described by the following mass balance:

$$\frac{dC_i}{dt} = v_{i, \text{dis}} \cdot \frac{A_{\text{dis}}}{V} \cdot R_{\text{dis}} \tag{6}$$

where C_i is the concentration of component i in the reactor (mol L⁻¹); t is time (s); $v_{i,\text{dis}}$ is the stoichiometric coefficient of i in the dissolution reaction; A_{dis} is the surface area (m²); V is the volume of the batch reactor (L); and R_{dis} is the dissolution rate (mol m⁻² s⁻¹). Rearranging Eq. (4) gives:

$$R_{\rm dis} \cdot v_{i,\rm dis} = \frac{dC_j}{dt} \cdot \frac{V}{A_{\rm dis}} \tag{7}$$

Typically, the dissolution rate in a batch experiment is obtained by measuring the concentration of component i at different times during the experiment and using Eq. (7). The hidden assumption in this calculation is that the change in concentration (ΔC_i) is linear with time during the sampling interval, and therefore the reaction rate may be readily calculated by substituting the average change in concentration with time ($\Delta C_i/\Delta t$) for the time derivative of the concentration (dC_i/dt) in Eq. (7).

If i is removed by precipitation of secondary phases, the resulting rate is the net rate of the release of i by dissolution minus its consumption by precipitation. Taking into account the effect of precipitation of secondary minerals, Eq. (6) should be rewritten as:

$$\frac{dC_i}{dt} = \frac{v_{i,\text{dis}} \cdot A_{\text{dis}} \cdot R_{\text{dis}} + v_{i,\text{pre}} \cdot A_{\text{pre}} \cdot R_{\text{pre}}}{V}$$
(8)

where $v_{i,pre}$ is the stoichiometric coefficient of i in the precipitation reaction; A_{pre} is the surface area (m²); and R_{dis} is the precipitation rate (mol m⁻² s⁻¹). Note that in our formalism, the rate is defined to be negative for precipitation and positive for dissolution, and hence the precipitation term is added to the dissolution term.

The net dissolution rate of a silicate mineral may be obtained by performing batch experiment with initial solution that contains isotopic spike. The main assumption in the following calculations is that fractionation during the dissolution of the primary mineral and precipitation of the secondary mineral is negligible. While previous studies (e.g., Douthitt, 1982; De La Rocha et al., 2000; Ziegler et al., 2005a,b; Georg et al., 2006a, 2007, 2009; Opfergelt et al., 2011, 2012) showed that fractionation probably occurs during precipitation, Gruber et al. (2013) demonstrated that the errors due to this assumption are much smaller than the uncertainties associated with the determination of the rate. The dissolution rate may be determined using mass balance equations that follow the change in isotopic composition of the solutions with time (Gruber et al., 2013):

$$R_{\text{dis}} = \frac{\begin{pmatrix} \frac{2^9 \text{Si}}{2^8 \text{Si}} \end{pmatrix}_t \cdot \frac{d^{28} \text{Si}}{dt} - \frac{d^{29} \text{Si}}{dt}}{\begin{pmatrix} \frac{2^9 \text{Si}}{2^8 \text{Si}} \end{pmatrix}_t \cdot \begin{pmatrix} \frac{2^8 \text{Si}}{10 \text{Tal} \text{Si}} \end{pmatrix}_{\text{dis}} - \begin{pmatrix} \frac{2^9 \text{Si}}{10 \text{Tal} \text{Si}} \end{pmatrix}_{\text{dis}} \end{pmatrix} \cdot \upsilon_{\text{Si,dis}} \cdot A_{\text{dis}}}$$
(9)

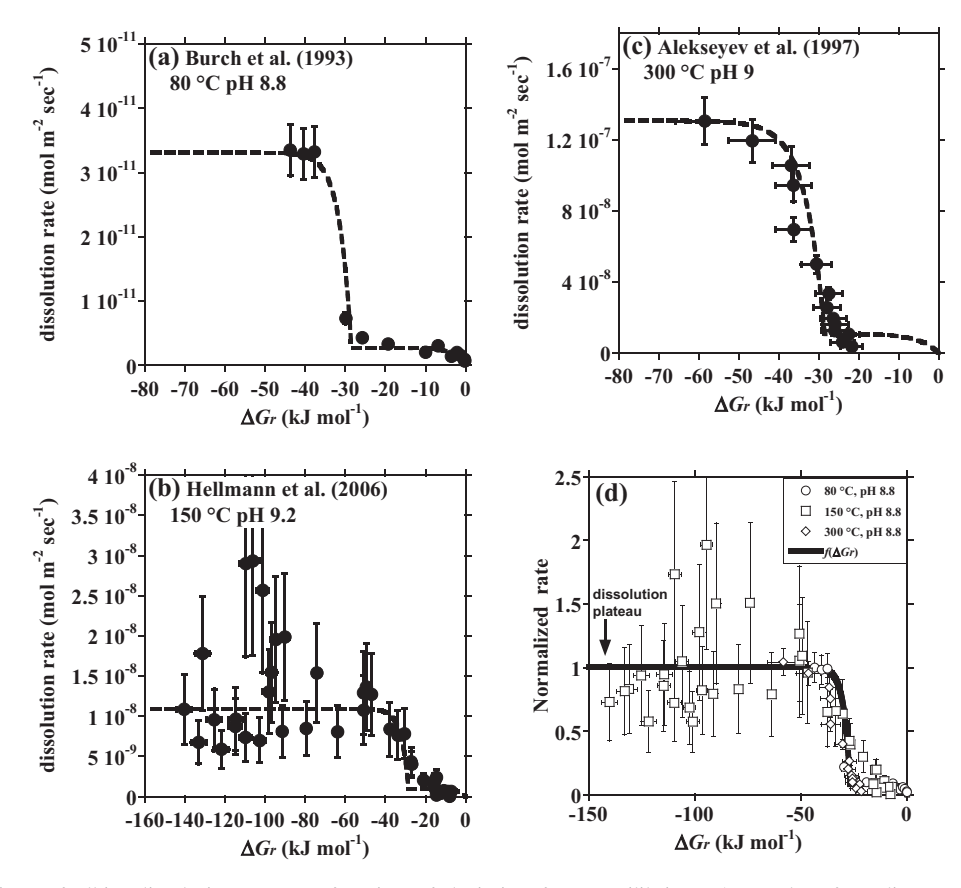


Fig. 1. Comparison of albite dissolution rates as function of deviation from equilibrium (ΔG_r) taken from literature data at various temperatures to the rate law of Eq. (5), where the dots are the experimental data at temperature of: (a) 80 (Burch et al., 1993); (b) 150 (Hellmann and Tisserand, 2006); and (c) 300 °C (Alekseyev et al., 1997). The dashed lines are the predicted dissolution rate of Eq. (5) where k_1 and k_2 equal: (a) $3.05 \cdot 10^{-11}$ and $2.73 \cdot 10^{-12}$ (mol m⁻² s⁻¹); (b) $1.00 \cdot 10^{-8}$ and $8.96 \cdot 10^{-10}$ (mol m⁻² s⁻¹); (c) $1.20 \cdot 10^{-7}$ and $1.08 \cdot 10^{-8}$ (mol m⁻² s⁻¹). $\Delta G_{crit} = -28.5$ kJ mol⁻¹ and B = 4. Sub-figure (d) shows the change in the normalized dissolution rate (dissolution rate divided by the plateau dissolution rate) at 80 (Burch et al., 1993), 150 (Hellmann and Tisserand, 2006) and 300 °C (Alekseyev et al., 1997) with deviation from equilibrium (ΔG_r). The solid line is a fitting of the rate law of Eq. (5) to the data at 80 °C. In all sub-figures error bars represent two standard deviations.

2. EXPERIMENTAL METHODS

2.1. Albite sample

The sample used in this study is the EVJE (Norway) albite from Ward's Scientific Est. The chemical composition of the albite sample was determined following digestion with lithium metaborate. Elemental concentrations were determined by Optima-5300 ICP-Atomic-Emission-Spectrometer and Perkin-Elmer ICP-MS. Each run included repeated determinations of international standards (NIM-L, NIM-G). The composition of the EVJE albite sample is Na_{0.99}Ca_{0.01}Al_{1.04}Si_{2.97}O₈ (chemical analysis of the sample is presented in Table 1). The isotopic composition of the silicon in EVJE albite is $\delta^{29} \text{Si}_{\text{NBS-28}} = 0.41\%$ and $\delta^{30} \text{Si}_{\text{NBS-28}} = 1.76\%$ $(^{29}\text{Si}/^{28}\text{Si} = 0.05065 \text{ and } ^{30}\text{Si}/^{28}\text{Si} = 0.03368)$. For further details on Si isotopes analyses see Section 2.6.

The albite was ground with an agate pestle and mortar and then sieved to particle size of 53–106 µm. Because the grains are often coated with sub-micron sized particles, the ground albite sample was ultrasonically rinsed with

Table 1 Chemical composition Evje albite (Norway).

%	Blank	Evje Norwa		
SiO ₂	0.5	67.2		
Al_2O_3	0.1	19.5		
Fe_2O_3	0.1	0.03		
TiO_2	0.01	< 0.01		
CaO	0.3	0.52		
MgO	< 0.1	< 0.01		
Na ₂ O		11.2		
K_2O		0.24		
SO_3	< 0.5			
P_2O_5	< 0.5			
Total		98.8		

ethanol eight times for about 20 min per treatment. The cleaned albite grains were then rinsed with deionized water and freeze-dried. Finally, the sample was kept in an oven at 105 °C overnight to exclude possible organic (Fu et al., 2009). In the following sections the term "untreated" albite sample refers to the mineral sample after sieving. The term

"treated" albite sample refers to mineral sample that was dissolved during a multi-point batch experiment under far-from-equilibrium conditions until dissolution rate was constant during a period of 13 days, as is described in Section 2.3.1.1 below.

2.2. Solutions

Two types of initial solutions were used in the present study: (a) Al, Na and Si free solutions for the far-from-equilibrium experiments; and (b) solutions spiked with silicon isotopes for the closer-to-equilibrium experiments.

Al, Na and Si free solutions were prepared from double deionized water (DDW) adjusted with trace metal grade HCl 4.5% to pH 5. Isotopically enriched solutions were prepared by dissolving two different SiO₂ powders (from Isoflex USA). One powder, which was enriched with ³⁰Si, was used in the experiment with the treated albite sample. A second powder, which was enriched with ²⁹Si, was used in the experiment with the untreated albite sample. Both powders were dissolved with Trace select grade KOH 30%. The pH of the spiked solutions was than reduced using trace metal grade HCl 4.5%.

2.3. Experimental setting

Two types of experiments were used: "single-point batch experiments" (several identical reactors, each reactor was used to determine one data point) and "multi-point batch experiments" (one reactor was sampled several times). The two single-point batch experiments were used to measure closer-to-equilibrium dissolution rates of treated and untreated albite samples by using spiked solution. One multi-point batch experiment was used to determine far-from-equilibrium dissolution rate and two others multi-point batch experiments were used to determine the change in surface reactivity. In all multi-point batch experiments the dissolution rates were derived using standard methods. List of experiments and conditions are written in Table 2.

2.3.1. Multi-point batch experiments

2.3.1.1. Treated far-from-equilibrium experiment. Untreated albite sample which was used previously in short, low temperature (\approx 3 °C) experiments (which is not described in the present study), was collected, filtered and dried, and subsequently used in a multi-point batch experiment. In this experiment. 10.25 ± 0.01 g albite was added 500.00 ± 0.01 g solution. During the entire experiment, the solution was under far-from-equilibrium conditions with respect to albite dissolution ($\Delta G_r \le -62.8 \text{ kJ mol}^{-1}$), i.e., within the dissolution plateau where dissolution rate is independent of deviation from equilibrium. It was conducted with solutions that initially contained no Al and no Si, and therefore the rate was determined using the standard method (Eq. (7)). After each sampling, the albite crystals were separated from most of the solution and a fresh solution was introduced into the reactor, in order to lower the concentrations of Al and Si. Therefore, the results are shown in terms of accumulated amounts of dissolved elements (Na, Al or Si) and not as concentrations (Table 3).

The dissolution rates were determined during the stage of constant Si (moles) release rate (starting about 24 h after the beginning of the experiment, Table 3). After about 13 days, the crystals were separated from the solution using a vacuum filter system with PVDF 0.22 µm filter papers. In order to avoid precipitation from the remaining solution during drying, the solution was removed by rinsing the wet crystals and the filter with 5 ml of double deionized water. Afterwards the treated albite crystals were dried in a desiccator at room temperature.

2.3.1.2. Far-from-equilibrium surface reactivity experiment. To determine the effect of surface reactivity, two multipoint batch experiments (B-1 and B-2) were conducted with untreated albite sample. The samples that were used in these experiments, and in the single-point batch experiments that was conducted with untreated albite, were taken from the same albite batch. 0.5000 ± 0.0001 g albite was added to $200.00 \pm 0.01\,\mathrm{g}$ solution (DDW adjusted with trace metal grade HCl 4.5% to pH 5). During the entire experiment, the solution was far-from-equilibrium with respect to albite dissolution ($\Delta G_r \le -62.8 \text{ kJ mol}^{-1}$), i.e., within the dissolution plateau where dissolution rate is independent of deviation from equilibrium. The solution was sampled using a logarithmic time schedule. Periodically, fresh solution was introduced into the reactor, in order to keep the experiment within the dissolution plateau. The experimental results and conditions are listed in Table 4.

2.3.2. Single-point batch experiments

Two sets of single-point batch experiments were conducted under closer-to-equilibrium conditions. Depending on the set, 25 or 14 identical bottles were placed together in a thermostatic bath, and each data point was obtained by stopping the reaction in one reactor. In each of the experiments 0.5000 ± 0.0001 (g) albite was added to 200.00 ± 0.01 (g) solution in 250 ml Polyethylene bottles and then placed in a rocking thermostatic water bath held at a constant temperature of 25 ± 0.1 °C. Solution sample (approximately 5 ml) was taken from the bottle and then filtered with PVDF 0.2 µm filter disk into a tube for pH measurement. The rest of the solution was separated from the solids using a vacuum filter system with PVDF 0.22 µm filter papers. An approximately 0.5 g trace metal grade HCl 4.5% solution was added to 89.5 g filtered solution to make the solution under saturated with respect to secondary phases. The compositions of the experimental solutions and their isotopic abundances are listed in Tables 5 and 6.

2.4. Bulk elemental concentration measurements

Total concentrations of Al and Si in solution were analyzed colorimetrically with Perkin Elmer Lambda 2S UV–visible spectrophotometer, using the Catechol violet method (Dougan and Wilson, 1974) and Molybdate blue method (Koroleff, 1976), respectively. The uncertainty in measured Al and Si was less than $\pm 5\%$ for concentrations above 4 μM . For Al, the uncertainty increased to $\pm 26\%$ for measurements at low concentrations of $0.5\,\mu M$.

Table 2 List of experiments and initial conditions.

Experiment	Section 2.3.2: untreated closer-to- equilibrium	Section 2.3.1.2: far- from-equilibrium surface reactivity B-1	Section 2.3.1.2: far- from-equilibrium surface reactivity B-2	Section 2.3.1.1: treated far-from- equilibrium	Section 2.3.2: treated closer-to- equilibrium
Type	Single-point batch experiment	Multi-point batch experiment	Multi-point batch experiment	Multi-point batch experiment	Single-point batch experiment
Chemical	31.3 μM Na,	No Si, Al and Na	No Si, Al and Na	No Si, Al and Na	32.61 μM Na,
composition of	0.80 μM Al,	addition. pH 5 adjusted	addition. pH 5 adjusted	addition, pH 5	0.38 μM Al,
the initial solution	39.65 μM Si, pH	by HCl	by HCl	adjusted by HCl	39.778 μM Si, pH
	5.28	•	•	•	5.09
Use of Si spike	Yes	No	No	No	Yes
solution					
Type of Si spike	²⁹ Si	_	_	_	³⁰ Si
Si initial isotopic	0.23% ²⁸ Si, 99.71%	_	_	_	0.40% ²⁸ Si, 0.05%
composition	²⁹ Si, 0.06% ³⁰ Si				²⁹ Si, 99.54% ³⁰ Si
Type of albite	Fresh	Fresh	Fresh	Fresh	Treated
Solution renewal	No	Yes	Yes	No	No
Solution renewal interval	No solution renewal	Every 4 samples	Every 4 samples	No solution renewal	No solution renewal

Table 3 Experimental conditions and results of the far-from-equilibrium experiment with treated albite sample. The uncertainty for the Gibbs free energy is $= +2.76 \\ -1.59$.

	-1.,									
Sample	Time (h)	Amount of dissolved Si (mol)	Amount of dissolved Al (mol)	Amount of dissolved Na (mol)	pН	Amount of dissolved albite (mol)	Dissolution rate (mol _{Ab} m ⁻² s ⁻¹)	Uncertainty on dissolution rate (2σ) (%)	ΔG_r albite (kJ mol ⁻¹)	Reactivity factor
0	0.0	0	0	0	4.86	0				
1	1.0	$1.59 \cdot 10^{-7}$	$1.08 \cdot 10^{-7}$	$3.51 \cdot 10^{-6}$	5.67	$5.32 \cdot 10^{-8}$	$1.95 \cdot 10^{-12}$	123	-69.05	3.82
2	2.9	$2.19 \cdot 10^{-7}$	$2.32 \cdot 10^{-7}$	$3.47 \cdot 10^{-6}$	5.00	$7.32 \cdot 10^{-8}$	$1.05 \cdot 10^{-12}$	18	-85.50	2.07
3	6.9	$3.83 \cdot 10^{-7}$	$5.65 \cdot 10^{-7}$	$3.71 \cdot 10^{-6}$	4.92	$1.27 \cdot 10^{-7}$	$8.38 \cdot 10^{-13}$	21	-80.84	1.64
4	23.4	$8.63 \cdot 10^{-7}$	$1.68 \cdot 10^{-6}$	$4.36 \cdot 10^{-6}$	5.11	$2.87 \cdot 10^{-7}$	$6.34 \cdot 10^{-13}$	33	-66.69	1.24
5	47.9	$1.34 \cdot 10^{-6}$	$2.66 \cdot 10^{-6}$	$4.77 \cdot 10^{-6}$	5.17	$4.48 \cdot 10^{-7}$	$5.37 \cdot 10^{-13}$	12	-64.67	1.05
6	72.4	$1.82 \cdot 10^{-6}$	$3.27 \cdot 10^{-6}$	$5.35 \cdot 10^{-6}$	5.06	$6.08 \cdot 10^{-7}$	$5.30 \cdot 10^{-13}$	12	-66.36	1.04
7	98.7	$2.33 \cdot 10^{-6}$	$3.90 \cdot 10^{-6}$	$5.67 \cdot 10^{-6}$	5.10	$7.76 \cdot 10^{-7}$	$5.89 \cdot 10^{-13}$	22	-66.38	1.15
8	121.7	$2.88 \cdot 10^{-6}$	$4.59 \cdot 10^{-6}$	$6.07 \cdot 10^{-6}$	5.09	$9.62 \cdot 10^{-7}$	$5.29 \cdot 10^{-13}$	42	-67.59	1.04
9	145.4	$3.23 \cdot 10^{-6}$	$5.00 \cdot 10^{-6}$	$6.32 \cdot 10^{-6}$	5.07	$1.07 \cdot 10^{-6}$	$4.69 \cdot 10^{-13}$	27	-70.17	0.92
10	168.1	$3.68 \cdot 10^{-6}$	$5.44 \cdot 10^{-6}$	$6.58 \cdot 10^{-6}$	5.04	$1.22 \cdot 10^{-6}$	$5.78 \cdot 10^{-13}$	16	-70.05	1.13
11	191.4	$4.20 \cdot 10^{-6}$	$5.82 \cdot 10^{-6}$	$6.89 \cdot 10^{-6}$	4.99	$1.40 \cdot 10^{-6}$	$4.96 \cdot 10^{-13}$	40	-71.77	0.97
12	215.9	$4.55 \cdot 10^{-6}$	$6.14 \cdot 10^{-6}$	$7.29 \cdot 10^{-6}$	5.01	$1.51 \cdot 10^{-6}$	$4.40 \cdot 10^{-13}$	24	-71.51	0.86
13	240.3	$4.99 \cdot 10^{-6}$	$6.50 \cdot 10^{-6}$	$7.52 \cdot 10^{-6}$	5.00	$1.66 \cdot 10^{-6}$	$4.89 \cdot 10^{-13}$	12	-71.36	0.96
14	266.4	$5.45 \cdot 10^{-6}$	$6.78 \cdot 10^{-6}$	$7.75 \cdot 10^{-6}$	4.99	$1.81 \cdot 10^{-6}$	$5.04 \cdot 10^{-13}$	14	-71.57	0.99
15	289.6	$5.90 \cdot 10^{-6}$	$7.01 \cdot 10^{-6}$	$7.98 \cdot 10^{-6}$	4.96	$1.96 \cdot 10^{-6}$	$5.67 \cdot 10^{-13}$	17	-73.71	1.11
16	311.4	$6.38 \cdot 10^{-6}$	$7.31 \cdot 10^{-6}$	$8.31 \cdot 10^{-6}$	4.93	$2.12 \cdot 10^{-6}$	$5.67 \cdot 10^{-13}$	12	-75.25	1.11

Detection limits for analyses of Al and Si are less than 0.5 $\mu M.$ Total Na and Ca were analyzed with Inductively Coupled Plasma Quadrupole Mass Spectrometer (ICP-QMS) Agilent 7700×. The concentrations were determined relative to calibration curves developed with synthetic multi-element standards that spanned the concentration range of interest. Lithium and Scandium were added to samples and standards to serve as the internal standards for normalization of analytical results. The uncertainty in measured Na and Ca is $\pm 10\%.$

The pH was measured at experimental temperature on a stirred aliquot of solution using a semi-micro 83-01 Orion Ross combination electrode. The reported accuracy is ± 0.02 pH units ($\pm 4.5\%$ in H^+ activities), and the precision is ± 0.10 pH units at pH ≈ 6 .

2.5. Surface area

The initial specific surface areas of the albite sample was measured by the Brunauer–Emmett–Teller (BET) method (Brunauer et al., 1938), using 5-points of N_2 adsorption isotherms, employing a Micromeritics Gemini II-2375 surface area analyzer and is equal to $0.330\pm0.039~\text{m}^2~\text{g}^{-1}$.

2.6. Silicon isotopes analyses

In order to reduce the concentrations of cations that might interfere with the isotopic analysis, all solutions were pretreated using the column method (Georg et al., 2006b) by filing 1.8 (ml) BIO-RAD AG 50W-X12 cation exchange resin in BIO-RAD Poly-Prep Chromatography Columns.

Then, the resin was cleaned by adding the following solutions: (1) 6 ml 3 N HCl; (2) 6 ml 6 N HCl; (3) 3 ml 10 N HCl; (4) 6 ml 6 N HCl; (5) 6 ml 3 N HCl; (6) 3 times 6 ml DDW. Following cleaning, a sample containing at least 1 µg Si was loaded, followed by 3.6 ml DDW.

Due to logistical reasons, samples from the experiment with the untreated albite sample were conducted using a spike solution enriched with ²⁹Si and were measured at Trent University while samples from the experiment with the treated albite sample were conducted using a spike solution enriched with ³⁰Si and were measured at Geological Survey of Israel.

2.6.1. Analyses of the samples from the closer-to-equilibrium untreated single-point batch experiment

The samples that were enriched in ²⁹Si (closer-to-equilibrium untreated single-point batch experiment) were analyzed by MC-ICP-MS (Thermo Fisher Neptune Plus) at Trent University, Water Quality Centre. To ensure the interference-free determination of the Si isotope masses, the instrument was set to operate in medium resolution $(R \sim 4500 \text{ taken as } dM/M \text{ at } 5\% \text{ and } 95\% \text{ peak-height}).$ The samples were introduced via an ApexQ sample introduction system (Elemental Scientific Inc.) at a flow rate of about 50 µl min⁻¹. The high-sensitivity (x-skimmer cone) was used in order to maximize instrument sensitivity $(\sim 30 \text{ V ppm}^{-1} \text{ Si}, 10^{11} \text{ ohm resistor})$. Prior to each sample a blank solution was measured and the background signals were subtracted from the subsequent sample measurements. Both sample and blank measurements consisted of 35 cycles with an integration time of 8.3 s each. Instrumental mass bias was corrected for by external normalization using Mg-standard (DSM-3) as internal standard (Bizzarro et al., 2011) and applying the mass-fractionation factor obtained from the Mg (f_{Mg}) to the Si measurements. The absolute Si isotope abundances (in %) were then computed from the mass-bias corrected Si mass ratios. Instrumental mass-bias is very stable and the long-term variability (>4 months) is <1%, so that f_{Mg} only shows minute variability between -1.507 and -1.523.

$$f_{\rm Mg} = \ln(^{j/24}R/^{j/24}r) / \ln(^{j}M/^{24}M)$$
 (10)

where j = 25 or 26, j/24R being the 'certified' j/25/24 Mg or j/26/24 Mg ratio for DSM-3 (Bizzarro et al., 2011) and j/26/24 being the absolute mass of j/25/26 Mg and 24-Mg.

2.6.2. Analyses of the samples from the closer-to-equilibrium treated single-point batch experiment

The samples that were enriched in ³⁰Si (treated single-point batch experiment) were analyzed by MC-ICP-MS (Nu Plasma II, UK) at the Geological Survey of Israel.

The instrument was set to operate in medium resolution ($R \sim 7000$ taken as dM/M at 5% and 95% peak-height). The samples were introduced via a DSN-100 sample introduction system (Nu instruments, UK) at a flow rate of about $100 \, \mu \, \text{min}^{-1}$. The sensitivity achieved was $\sim 3 \, \text{V ppm}^{-1} \, ^{28} \text{Si}$ (for natural isotope composition of Si). Prior to each sample a blank solution was measured and the background signals were subtracted from subsequent sample measurements. Both sample and blank

measurements consisted of 15 cycles with an integration time of 10 s each.

To verify the method, sample of Amelia Court House albite was measured relative to NBS-28. The $\delta^{29}Si_{NBS-28}$ $(-0.27\pm0.27\%_o)$ and $\delta^{30}Si_{NBS-28}$ $(-0.44\pm0.20\%_o)$ of Amelia Court House albite were identical (within stated precision) to the reported values $(\delta^{29}Si_{NBS-28}=-0.11\%_o$ and $\delta^{30}Si_{NBS-28}=-0.256\%_o)$ by Gruber et al. (2013).

Isotopic ratios of Si of all solutions were measured with a Nu multi-collector inductively coupled plasma mass spectrometer (MC-ICP-MS) using standard bracketing method. The Si isotope standards BGU-30 (0.6121% ²⁸Si, 0.679% ²⁹Si and 99.32% ³⁰Si) was used as the bracketing standard for all samples, and provides the zero point reference for the "delta scale". Due to the significant difference between the isotopic composition of the measured samples (more than 90% 30Si) and of the NBS-28 standard (about 92.23% ²⁸Si), NBS-28 should not be used as the bracketing standard. It has been shown (Malinovsky et al., 2003; Halicz et al., 2008) that concentration of analytes in solution can influence the measured isotopic ratio. A high difference in isotopic composition such as in the case of NBS-28 and the samples leads to high difference in the concentration of the individual isotopes, which causes a variance in the measures isotopic ratio. The bracketing standard, BGU-30, was prepared by dissolving SiO₂ powder enriched with 30Si (from Isoflex USA) with Trace select grade KOH 30%. The pH of the standard solution was than reduced using trace metal grade HCl 4.5% to about 5. In order to constrain precisely the isotopic composition of the standard, two mixtures were prepared from the standard solution with silicon ICP standard solution. As the relative amount of the silicon ICP standard in the mixtures was 95% and 97.5%, it is possible to measure the isotopic composition of the mixtures using the NBS-28 as the bracketing standard. In a similar concept to the isotope dilution method, it's possible to use set of mass balance equations in order to calculate the isotopic composition and concentration of the isotopic enriched standard. The precision on the isotopic composition and Si concentration between the two mixtures was better than 0.0013%. To examine the precision of the analyses, an internal Si isotope standard, ISTD-30, was measured multiple times during the analytical session, giving an average δ³⁰Si_{BGU-30} value of $-602.65 \pm 4\%$ and $\delta^{29} Si_{BGU-30}$ value of $-224.28 \pm 7\%$. The uncertainty (2σ) in measured isotopic ratios using this method is $\pm 0.02\%$.

2.7. Thermodynamic calculations

Ion activities and degrees of saturation were calculated with the geochemical speciation software PHREEQC 2.18.3 (Parkhurst and Appelo, 1999) using the extended Debye–Hückel equation and Zhu et al. (2010) thermodynamic data set. The uncertainty in ΔG_r was estimated by calculating the uncertainty on the IAP (Ion Activity Product) of albite using Gaussian error propagation (Barrante, 1974) that is directly influenced by the uncertainty on the ion concentration measurements.

Table 4
Experimental conditions and results of the reactivity experiment.

Sample	Time	Si	Al	Albite	Uncertainty in	Albite	Reactivity	Sample	Time	Si	Al	Albite	Albite	Uncertainty in	Reactivity
Bumpie	(h)	(μ M)	(μ M)	dissolution rate	dissolution rate	dissoloved	factor	Sumple	(h)	(µM)	(µM)	dissolution rate	dissoloved	dissolution rate	factor
	()	(,,-,-)	(1)	$(\text{mol}_{Ab} \text{ s}^{-1} \text{ g}_{Ab}^{-1})$	(2σ) (%)	(mol)			()	(1)	()	$(\text{mol}_{Ab} \text{s}^{-1} \text{g}_{Ab}^{-1})$	(mol)	(2σ) (%)	
B-1 0	0	0.000				0		B-2 0	0	0.000		. 110 2.110/	0		
B-1 1	1	0.145		$2.20 \cdot 10^{-12}$	45.6	$9.68 \cdot 10^{-9}$	80.96	B-2 1	1	0.244		$3.59 \cdot 10^{-12}$	$1.62 \cdot 10^{-8}$	47.9	113.07
B-1 2	3	0.216		$6.28 \cdot 10^{-13}$	17.9	$1.35 \cdot 10^{-8}$	23.04	B-2 2	3	0.347		$8.44 \cdot 10^{-13}$	$2.14 \cdot 10^{-8}$	20.3	26.54
B-1 3	8	0.333		$3.31 \cdot 10^{-13}$	11.7	$1.83 \cdot 10^{-8}$	12.15	B-2 3	8	0.514		$4.01 \cdot 10^{-13}$	$2.78 \cdot 10^{-8}$	14.3	12.63
B-1 4	27	0.681				$2.83 \cdot 10^{-8}$		B-2 4	27	0.973			$3.96 \cdot 10^{-8}$		
B-1 5	28	0.164		$2.88 \cdot 10^{-13}$	42.9	$2.82 \cdot 10^{-8}$	10.59	B-2 5	28	0.164		$7.58 \cdot 10^{-13}$	$3.76 \cdot 10^{-8}$	87.4	23.85
B-1 6	30	0.192		$2.57 \cdot 10^{-13}$	16.3	$2.97 \cdot 10^{-8}$	9.45	B-2 6	30	0.260		$3.88 \cdot 10^{-13}$	$4.28 \cdot 10^{-8}$	68.7	12.20
B-1 7	36	0.249		$1.90 \cdot 10^{-13}$	3.7	$3.20 \cdot 10^{-8}$	6.98	B-2 7	36	0.296		$1.99 \cdot 10^{-13}$	$4.43 \cdot 10^{-8}$	8.0	6.29
B-1 8	54	0.444				$3.79 \cdot 10^{-8}$		B-2 8	54	0.526			$5.12 \cdot 10^{-8}$		
B-1 9	55	0.112		$1.12 \cdot 10^{-13}$	80.4	$3.76 \cdot 10^{-8}$	4.11	B-2 9	55	0.145		$1.08 \cdot 10^{-13}$	$5.16 \cdot 10^{-8}$	26.4	4.77
B-1 10	57	0.126		$1.99 \cdot 10^{-13}$	1.9	$3.84 \cdot 10^{-8}$	7.30	B-2 10	56	0.152		$1.70 \cdot 10^{-13}$	$5.20 \cdot 10^{-8}$	9.4	5.37
B-1 11	62	0.173		$1.66 \cdot 10^{-13}$	4.0	$4.03 \cdot 10^{-8}$	6.12	B-2 11	62	0.197		$1.91 \cdot 10^{-13}$	$5.39 \cdot 10^{-8}$	0.5	6.01
B-1 12	80	0.347				$4.55 \cdot 10^{-8}$		B-2 12	80	0.402			$6.01 \cdot 10^{-8}$		
B-1 13	123	0.244		$1.28 \cdot 10^{-13}$	2.1	$5.58 \cdot 10^{-8}$	4.69	B-2 13	123	0.270		$1.36 \cdot 10^{-13}$	$7.10 \cdot 10^{-8}$	1.6	4.29
B-1 14	174	0.465		$1.19 \cdot 10^{-13}$	2.1	$6.70 \cdot 10^{-8}$	4.37	B-2 14	174	0.496		$1.26 \cdot 10^{-13}$	$8.31 \cdot 10^{-8}$	3.2	3.96
B-1 15	226	0.727		$1.04 \cdot 10^{-13}$	6.7	$7.79 \cdot 10^{-8}$	3.81	B-2 15	226	0.771		$1.15 \cdot 10^{-13}$	$9.44 \cdot 10^{-8}$	2.1	3.63
B-1 16	272	0.995				$8.54 \cdot 10^{-8}$		B-2 16	272	1.087			$1.03 \cdot 10^{-7}$		
B-1 17	444	0.654		$8.63 \cdot 10^{-14}$	3.9	$1.13 \cdot 10^{-7}$	3.17	B-2 17	444	0.703		$9.07 \cdot 10^{-14}$	$1.32 \cdot 10^{-7}$	1.9	2.85
B-1 18	603	1.075		$7.54 \cdot 10^{-14}$	3.5	$1.36 \cdot 10^{-7}$	2.77	B-2 18	603	1.165		$8.34 \cdot 10^{-14}$	$1.57 \cdot 10^{-7}$	2.6	2.62
B-1 19	777	1.602		$6.79 \cdot 10^{-14}$	2.8	$1.59 \cdot 10^{-7}$	2.49	B-2 19	777	1.765		$7.79 \cdot 10^{-14}$	$1.82\cdot 10^{-7}$	1.4	2.45
B-1 20	941	2.238				$1.78 \cdot 10^{-7}$		B-2 20	941	2.542			$2.05 \cdot 10^{-7}$		
B-1 21	1664	1.759		$4.88 \cdot 10^{-14}$	10.4	$2.56 \cdot 10^{-7}$	1.79	B-2 21	1664	2.019		$5.80 \cdot 10^{-14}$	$2.97 \cdot 10^{-7}$	10.1	1.83
B-1 22	2719	3.245	1.16	$3.98 \cdot 10^{-14}$	4.0	$3.36 \cdot 10^{-7}$	1.46	B-2 22	2719	3.789	1.28	$4.70 \cdot 10^{-14}$	$3.92 \cdot 10^{-7}$	4.8	1.48
B-1 23	3390	4.352	1.46	$3.01 \cdot 10^{-14}$	11.6	$3.79 \cdot 10^{-7}$	1.10	B-2 23	3389	5.012	1.44	$3.73 \cdot 10^{-14}$	$4.43 \cdot 10^{-7}$	6.7	1.18
B-1 24	4042	5.391	1.29			$4.07 \cdot 10^{-7}$		B-2 24	4042	6.353	1.40		$4.81 \cdot 10^{-7}$		
B-1 25	4707	1.742	0.70	$2.89 \cdot 10^{-14}$	3.6	$4.44 \cdot 10^{-7}$	1.06	B-2 25	4707	2.087	1.09	$3.21 \cdot 10^{-14}$	$5.20 \cdot 10^{-7}$	0.6	1.01
B-1 26	5453	2.408	0.96	$2.72 \cdot 10^{-14}$		$4.81 \cdot 10^{-7}$	1.00	B-2 26	5453	2.876	0.76	$3.18 \cdot 10^{-14}$	$5.63 \cdot 10^{-7}$		1.00

Table 5 Experimental conditions and results of the closer-to-equilibrium experiment with the untreated albite crystals. For the Gibbs free energy is $= \frac{+1.59}{-0.56}$.

•					*		1			•		-0.56		
Sample	Time (h)	Si MB ^a (μM)	Si IR ^b (μM)	²⁹ Si/ ²⁸ Si	³⁰ Si/ ²⁸ Si	Al (μM)	Na (μM)	pН	ΔG_r albite (kJ mol ⁻¹)	ΔG_r kaolinite (kJ mol ⁻¹)	ΔG_r gibbsite (kJ mol ⁻¹)	Dissolution rate (mol m ⁻² s ⁻¹)	Albite dissoloved (mol)	2σ dissolution rate uncertainty (%)
)A	0.0	39.65	39.65	424.811	0.25440	0.80	31.3	5.28	-32.25	25.36	-0.67		0	
В	0.25	39.03	40.02	90.198	0.07887	0.97	33.3	5.28	-31.56	26.36	-0.41	$8.50 \cdot 10^{-11}$	$2.50 \cdot 10^{-8}$	13
	0.6	38.87	40.06	84.307	0.07625	1.00	34.3	5.30	-31.09	26.90	-0.28	$3.91 \cdot 10^{-11}$	$2.72 \cdot 10^{-8}$	43
	0.9	39.39	40.11	76.172	0.07303	1.04	35.2	5.22	-32.22	25.42	-0.67	$1.21 \cdot 10^{-11}$	$3.08 \cdot 10^{-8}$	19
	1.4	39.34	40.16	70.470	0.06776	1.02	35.9	5.18	-32.87	24.46	-0.96	$1.08 \cdot 10^{-11}$	$3.38 \cdot 10^{-8}$	17
R	2.0	38.98	40.18	67.819	0.06777	1.07	36.2	5.23	-31.90	25.79	-0.57	$1.26 \cdot 10^{-11}$	$3.54 \cdot 10^{-8}$	18
В	2.7	38.92	40.25	61.130	0.06367	1.11	36.3	5.25	-31.45	26.41	-0.41	$9.31 \cdot 10^{-12}$	$4.00 \cdot 10^{-8}$	21
	3.5	39.42	40.37	52.132	0.06029	1.27	37.0	5.22	-31.54	26.45	-0.40	$6.21 \cdot 10^{-12}$	$4.81 \cdot 10^{-8}$	28
	5.8	39.78	40.45	47.765	0.05762	1.33	36.9	5.19	-31.94	26.02	-0.51	$3.56 \cdot 10^{-12}$	$5.31 \cdot 10^{-8}$	34
0	8.0	39.33	40.48	46.120	0.05685	1.25	37.1	5.16	-32.57	25.05	-0.79	$2.81 \cdot 10^{-12}$	$5.53 \cdot 10^{-8}$	20
1A	10.5	39.25	40.49	45.336	0.05637	1.43	37.0	5.24	-30.90	27.48	-0.16	$3.12 \cdot 10^{-12}$	$5.63 \cdot 10^{-8}$	18
2	13.1	38.98	40.61	40.571	0.05412	1.05	37.6	5.21	-32.11	25.31	-0.72	$2.29 \cdot 10^{-12}$	$6.37 \cdot 10^{-8}$	14
3	17.1	39.31	40.71	36.963	0.05219	1.20	37.2	5.28	-30.64	27.47	-0.16	$1.90 \cdot 10^{-12}$	$7.06 \cdot 10^{-8}$	16
8	48.9	39.74	41.20	25.940	0.04626	1.40	36.9	5.24	-31.83	26.15	-0.51	$1.64 \cdot 10^{-12}$	$1.04 \cdot 10^{-7}$	14
9	66.4	39.71	41.32	24.182	0.04567	1.69	37.5	5.27	-30.31	28.40	0.03	$1.51 \cdot 10^{-12}$	$1.12 \cdot 10^{-7}$	14
1 A	100.0	38.48	41.75	19.502	0.04322	1.76	37.4	5.40	-29.64	29.29	0.20	$1.11 \cdot 10^{-12}$	$1.40 \cdot 10^{-7}$	15
2	112.3	40.49	41.83	18.795	0.04275	1.84	37.3	5.41	-27.52	32.06	0.70	$9.34 \cdot 10^{-13}$	$1.46 \cdot 10^{-7}$	16
4	178.9	40.41	42.30	15.600	0.04104	1.97	37.0	5.40	-27.14	32.64	0.79	$7.53 \cdot 10^{-13}$	$1.77 \cdot 10^{-7}$	13
5	228.6	41.21	42.54	14.386	0.04049	2.21	38.0	5.38	-26.90	33.05	0.85	$7.71 \cdot 10^{-13}$	$1.92 \cdot 10^{-7}$	13
6	299.7	40.97	42.92	12.739	0.03967	1.95	37.4	5.44	-27.48	32.10	0.69	$7.48 \cdot 10^{-13}$	$2.18 \cdot 10^{-7}$	12
7	347.3	41.67	43.28	11.541	0.03905	2.06	37.6	5.54	-26.37	33.52	0.90	$7.18 \cdot 10^{-13}$	$2.42 \cdot 10^{-7}$	13
8	468.1	42.29	43.94	9.7956	0.03812	2.03	37.6	5.49	-24.89	35.20	1.14	$6.68 \cdot 10^{-13}$	$2.86 \cdot 10^{-7}$	13
9	573.3	43.13	44.41	8.8665	0.03752	2.13	38.5	5.61	-25.32	34.67	1.05	$4.05 \cdot 10^{-13}$	$3.17 \cdot 10^{-7}$	17
0	740.9	44.58	45.21	7.6142	0.03698	2.34	37.8	5.63	-23.37	37.14	1.37	$3.71 \cdot 10^{-13}$	$3.71 \cdot 10^{-7}$	12
1	1406.5	44.73	46.74	6.0065	0.03620	2.37	38.4	5.62	-22.79	37.66	1.41	$3.49 \cdot 10^{-13}$	$4.73 \cdot 10^{-7}$	13

a Molybdate Blue method.b Isotope Ratio method.

Table 6 Experimental conditions and results of the closer-to-equilibrium experiment with the treated albite crystals. For the Gibbs free energy is $= {+1.59 \atop -0.56}$.

Sample	Time (h)	Si (µM)	²⁹ Si/ ²⁸ Si	³⁰ Si/ ²⁸ Si	Al (μM)	Na (μM)	pН	ΔG_r albite (kJ mol ⁻¹)	Dissolution rate (mol m ⁻² s ⁻¹)	Albite dissoloved (mol)	2σ dissolution rate uncertainty(%)
0	0	39.778	0.1326	247.7	0.380	32.61	5.09	-37.29		0	
1	0.5	39.786	0.1276	236.0	0.280	28.01	4.88	-37.26	$7.15 \cdot 10^{-13}$	$5.77 \cdot 10^{-10}$	47
2	1.0	39.810	0.1467	208.5	0.281	27.39	4.86	-37.19	$7.16 \cdot 10^{-13}$	$2.19 \cdot 10^{-9}$	47
3	1.6	39.788	0.1235	233.5	0.285	29.12	4.81	-37.26	$5.67 \cdot 10^{-13}$	$7.06 \cdot 10^{-10}$	20
4	3.0	39.822	0.1187	197.2	0.308	27.29	4.77	-37.15	$3.16 \cdot 10^{-13}$	$2.99 \cdot 10^{-9}$	18
5	5.8	39.816	0.1199	202.6	0.318	29.61	4.74	-37.17	$2.44 \cdot 10^{-13}$	$2.59 \cdot 10^{-9}$	16
6	16.6	39.847	0.1092	177.1	0.206	28.94	4.79	-37.08	$1.97 \cdot 10^{-13}$	$4.65 \cdot 10^{-9}$	12
7	31.6	39.865	0.0997	164.3	0.344	30.14	4.77	-37.02	$1.60 \cdot 10^{-13}$	$5.92 \cdot 10^{-9}$	12
8	56.2	39.911	0.1020	139.9	0.339	29.12	4.78	-36.89	$1.25 \cdot 10^{-13}$	$8.99 \cdot 10^{-9}$	12
9	96.9	39.948	0.0934	124.8	0.365	31.84	4.82	-36.79	$1.12 \cdot 10^{-13}$	$1.15 \cdot 10^{-8}$	11
10	174.8	40.025	0.0911	102.1	0.326	28.79	4.76	-36.60	$9.91 \cdot 10^{-14}$	$1.66 \cdot 10^{-8}$	12
11	323.7	40.166	0.0920	76.47	0.455	30.42	4.81	-36.26	$7.43 \cdot 10^{-14}$	$2.61 \cdot 10^{-8}$	16
12	576.7	40.369	0.0886	56.19	0.372	29.71	4.83	-35.19	$6.99 \cdot 10^{-14}$	$3.97 \cdot 10^{-8}$	12
13	1008.6	40.553	0.0749	45.29			4.82			$5.22 \cdot 10^{-8}$	

3. RESULTS

3.1. Closer-to-equilibrium experiment with untreated albite crystals

Traditional methods use the change in concentration of the major ions (e.g., Si) that are released from the primary minerals to calculate dissolution rates. When rates determined by using traditional methods, the accuracy and precision of the obtained rates are limited by the absolute analytical uncertainty on the concentration measurements (Ganor et al., 2007; Gruber et al., 2013). Therefore, the major analytical challenge in measuring dissolution rates of silicate minerals at ambient temperature under closer-to-equilibrium conditions is to determine a small change in relatively high concentration. It is important to emphasize that the challenge is not to measure concentration of a few micro molars but to measure a change in concentration that is lower than the uncertainty on the

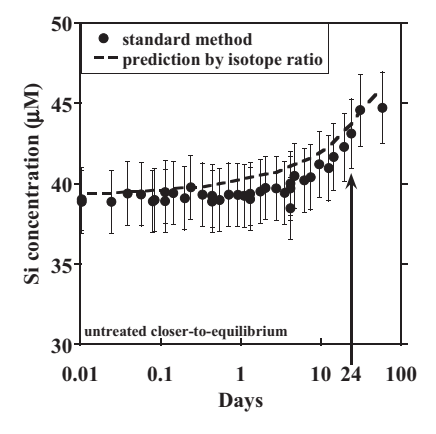


Fig. 2. The change with time in silicon concentration during untreated closer-to-equilibrium albite dissolution experiment. Error bars represent relative error of $\pm 4\%$ (2σ). The dashed line is the prediction of Si concentration based on the change of $^{29}\text{Si}/^{28}\text{Si}$ in solution.

ion concentration measurement. Fig. 2 shows the change in Si concentration measured by the molybdate blue method with time during dissolution experiment (Table 5) of the untreated albite crystals (black dots). During the first 24 days, the measured silicon concentration did not change within analytical uncertainty. Therefore, it is not possible to use these data to calculate the change in dissolution rate during the development of the experiment. In contrast to the Si concentration measurements, the ²⁹Si/²⁸Si ratio (Fig. 3) change significantly after 15 min, thus making the derivation of extremely slow dissolution rates possible. The change in total silicon concentration was calculated independently using the change in isotope composition and the concentration analysis (dashed line Fig. 2) and is in agreement with the measured Si concentrations. The dissolution during the experiment was congruent within uncertainty.

Dissolution rates during the experiment progress were calculated based on the change in isotopic composition with

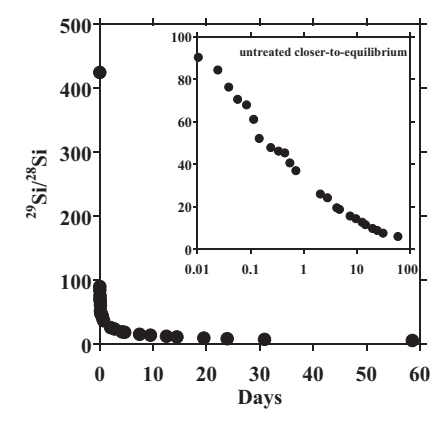


Fig. 3. The change with time in $^{29}\text{Si}/^{28}\text{Si}$ during the untreated closer-to-equilibrium albite dissolution closer-to-equilibrium experiment. Error bars are smaller than symbol size ($\pm 0.005\%$, two standard deviations). The insert is the same plot with a logarithmic X axis.

time using Eq. (9). With time, the dissolution rate decreases by about 2.5 orders of magnitude (Fig. 4).

3.2. Far-from-equilibrium surface reactivity experiment

In the previous experiment, the dissolution rate of albite decreases with time due to the decrease in the degree of undersaturation and due to the decrease in surface reactivity as more reactive particles and sites are extinct. In order to quantify the vital effect of the change in surface reactivity, another series of experiments were conducted with solutions that initially contain no Al and no Si, and therefore the rate may be determined using the standard method. Periodically, fresh solution was introduced into the reactor (to replace the sampled solution), in order to lower the concentrations of Al and Si (separating lines in Table 4). Due to the solution refreshments, the dissolution rate is not calculated by the time derivative of the Si concentration but by the time derivative of the cumulative amount (moles) of dissolved albite. As these experiments were conducted under far-from-equilibrium conditions (i.e., at the dissolution plateau), the decrease in dissolution rate in these experiments is independent of the degree of saturation, and is solely attributed to the change in mineral reactivity. Fig. 5 shows the change in Si concentration with time during the first 40 days of experiment B-2. Before the first solution replenishment, the change in Si concentration is parabolic due to the initial rapid change in dissolution rate (circles). After the first solution replenishment, the change in Si concentration becomes close to linear (squares) and remains close to linear following the second and the third refreshments (diamonds and triangles, respectively). During the course of the experiment, the dissolution rate was decreased by two orders of magnitude (Table 4). The rate continues to decrease even after more than half a year. The relative reactivity factor, defined as the ratio of the measured dissolution rate (mol g⁻¹ s⁻¹) divided by the

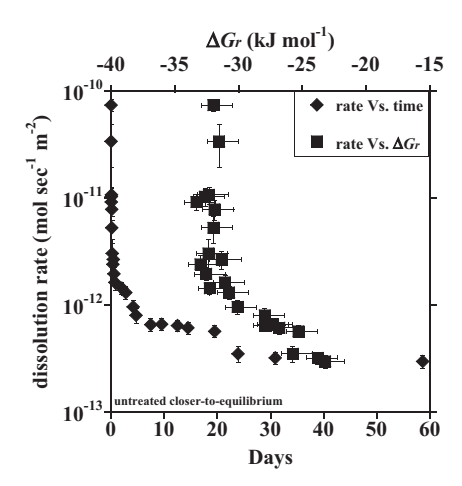


Fig. 4. The change with time (diamonds, lower x axis) and deviation from equilibrium (ΔG_r , squares, upper x axis) of dissolution rates of the untreated closer-to-equilibrium albite sample. The vertical and horizontal error bars represent two standard deviation uncertainties on dissolution rate and on ΔG_r value.

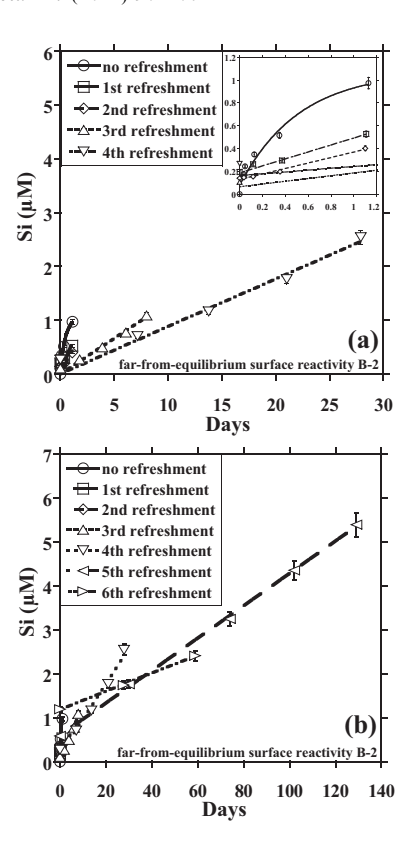


Fig. 5. The change in Si concentration (μM) with time during the far-from-equilibrium surface reactivity experiment B-2. Error bars represent uncertainty of $\pm 4\%$ (two standard deviations). (a) The first 39 days of the experiment; and (b) the entire experiment duration (227 days). The circles represents the initial dissolution (before any solution refreshment), squares – after the first solution refreshment, diamonds – after the second solution refreshment, and triangles – after the third solution refreshment. The insert is an enlargement of the first day of each stage.

dissolution rate after 227 days, was calculated for each time interval of the experiment. Fig. 6 shows the change in reactivity factor as a function of the amount of dissolved albite during experiments B-1 and B-2. During the initial stage of dissolution, both experiments show sharp decrease in reactivity with the amount of dissolved albite, while thereafter much more albite must be dissolved to change the reactivity. The data of both experiments may be described (lines in Fig. 6) with the following empirical power law:

$$R.F. = m_1 \times \text{mol}_{Ab}^{m_2} \tag{11}$$

where m_1 and m_2 are empirical parameters that were fitted to the experimental data and mol_{Ab} is the amount of dissolved albite (moles). The two experiments were fitted with different fitting parameters ($m_1 = 2.52 \cdot 10^{-6}$, $m_2 = -0.877$ for B-1 and $m_1 = 3.01 \cdot 10^{-7}$, $m_2 = -1.025$ for B-2). As the same solution was used in the two experiments, we conclude that the significant difference in rate indicates that the two albite sub samples that were used in those experiments had different initial surface reactivity, even though they were sampled from the same batch and were prepared together. It is suggested that the initial surface reactivity is influenced by small amounts (32.0 and 44.3 nmol during

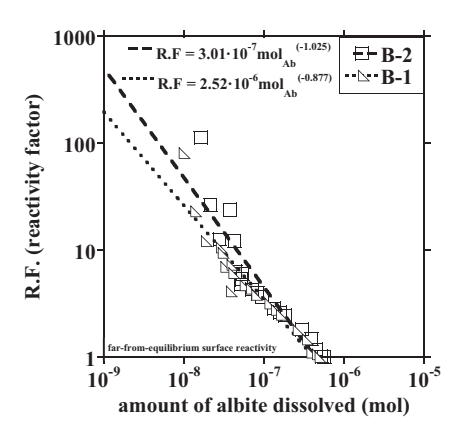


Fig. 6. The change in reactivity factor as a function of the amount of dissolved albite (mol). The squares (far-from-equilibrium surface reactivity experiment B-2) and triangles (far-from-equilibrium surface reactivity experiment B-1) are the experimental data. The dashed lines are curves that are fitted to each experimental data set using a power law.

the first 36 h of B-1 and B-2, respectively) of very reactive fine particles, in accordance with the suggestion of (Holdren and Berner, 1979) that feldspar dissolution in laboratory experiments is initially dominated by dissolution of ultrafine particles which are produced during grinding of the sample. Therefore, it is not possible to use any universal empirical fit of the data in order to differentiate between the effect of surface reactivity and the effect of deviation from equilibrium on the dissolution rates that was measured in the single-point batch experiment with the untreated albite crystals under closer-to-equilibrium conditions.

3.3. Treated far-from-equilibrium experiment

As the initial surface reactivity is a unique property of the sub sample and the amount of dissolved mineral, it would be possible to uniquely relate changes in dissolution rate to the effect of deviation from equilibrium only after: (i) decreasing the change in surface reactivity during the experiment; and (ii) reducing the variety in surface reactivity within the sample batch. In order to minimize the effect of change in the mineral surface reactivity on the measured dissolution rate, another multi-point batch experiment (Table 3) was conducted under far-from-equilibrium conditions. This experiment had two goals: (i) to prepare a large batch of sample (\approx 10 g) of treated sample in which the reactivity will remain constant within the time scale of a closer-to-equilibrium single-point batch experiment; and (ii) to measure the far-from-equilibrium dissolution rate of this batch. In this experiment, after each sampling, the solution inside the batch was replaced by a fresh solution. Consequently, the Si, Al and Na concentration were reduced and solution was kept under far-from-equilibrium conditions. In this experiment, the reactivity factor decreased by a factor of about 3.8 during the first day of the experiment (Table 3). After the first day, the reactivity factor remains constant within uncertainty for the next 12 days. Fig. 7 shows the measured dissolution rates during these 12 days as a function of deviation from equilibrium

 (ΔG_r) . Within the uncertainty on the measured dissolution rate, all the measured rates representing a constant dissolution rate of $5.33 \cdot 10^{-13}$ (mol m⁻² s⁻¹) $\pm 20\%$ (2 σ) for ΔG_r range values of -64.68 to -75.23 (kJ mol⁻¹).

3.4. Closer-to-equilibrium with treated albite crystals experiment

After reducing most of the surface reactivity during the far-from-equilibrium experiment, a single-point batch experiment with the "treated" crystals was conducted using spiked solution (enriched with ³⁰Si). As in the experiment with the untreated albite crystals, the spiked experimental solution became enriched in ²⁸Si with time due to dissolution of the albite sample, leading to decrease in the ³⁰Si/²⁸Si ratio (Table 6). Measuring the dissolution rate by tracking the change in Si isotope ratio is not compromised by secondary phase precipitation unlike other methods that derive reaction rates using concentrations differences over time (Gruber et al., 2013). Fig. 8 shows the change in dissolution rate with time and as a function of deviation from equilibrium. Two aspects are noteworthy: (1) As this experiment was conducted with treated albite sample, most of the change in dissolution rate is due to the change in the degree of undersaturation with respect to albite and therefore the dissolution rates spanned over about one order of magnitude instead of about three as in the experiment with the untreated crystals sample (Fig. 4); (2) The analytical noise is lower than that in the experiment with the untreated crystals sample. This observation is explained by the higher similarity between the albite samples that were introduced to each reactor in the former, as all crystals were treated simultaneous. The difference in reactivity of the untreated samples is also demonstrated in the reactivity experiments B-1 and B-2.

Although much of the excess reactivity was removed during treatment, a priory one cannot rule out the possibility that a further decrease in reactivity occurred during the experiment. As we showed above (Section 3.2), it is not

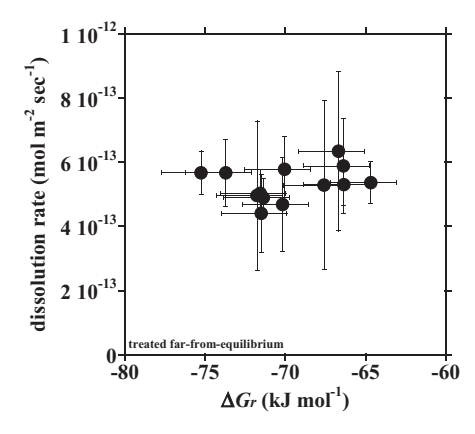


Fig. 7. Dissolution rate of the treated far-from-equilibrium albite sample as function of deviation from equilibrium ΔG_r under far-from-equilibrium conditions. The vertical and horizontal error bars represent two standard deviations uncertainties on dissolution rate and on ΔG_r value.

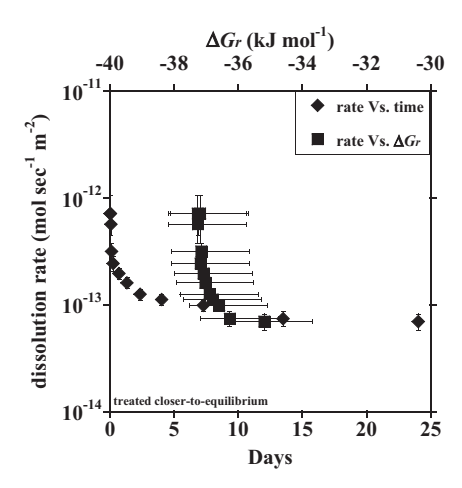


Fig. 8. The change with time (diamonds, lower x axis) and deviation from equilibrium (ΔG_r , squares, upper x axis) of dissolution rates of the treated closer-to-equilibrium albite sample. The vertical and horizontal error bars represent two standard deviations uncertainties on dissolution rate and on ΔG_r value.

possible to use any universal empirical fit of the data in order to differentiate between the effect of surface reactivity and the effect of deviation from equilibrium. Regardless, one can fit the results of the far-from-equilibrium experiment that was used to treat the sample to Eq. (11), in order to estimate the change in the reactivity factor during the closer-to-equilibrium experiment with the treated albite sample (Fig. 9). The extrapolation of the empirical power law indicates that during the entire closer-to-equilibrium experiment the reactivity factor decreased by only 7%.

4. DISCUSSION

4.1. The ΔG_r function

The combined rate low (Eq. (5)) includes the assumption that the overall dissolution rate is a sum of two different independent dissolution mechanisms and that the $f(\Delta G_r)$ is a continues function. This assumption contradicts the suggestion of Luttge (2006) and Arvidson and Luttge (2010) that the $f(\Delta G_r)$ has discontinuity between the two dissolution mechanisms and that when one mechanism operates, the second mechanism is switched off. The discontinuity function was proposed to explain different paths of the $f(\Delta G_r)$ in the transition ΔG_r range between the two mechanisms that were observed in different experiments (Beig and Luttge, 2006). The variations of $f(\Delta G_r)$ -rate can be also attributed to other factors such as: (i) the mineral surface history; (ii) solid/solution ratio; and (iii) the rate that the etch pits disappear when solution approach equilibrium or opening when solution deviates from equilibrium (Beig and Luttge, 2006). It's important to note there is no theoretical nor experimental evidence that would indicate the first mechanism (Eq. (1)) to cease under far-from-equilibrium conditions' as the stepwave model describes dissolution only at etch pits (Lasaga and Luttge, 2001). This issue is not yet resolved and is still under discussion. Both options may be used to predict the dissolution rate and to

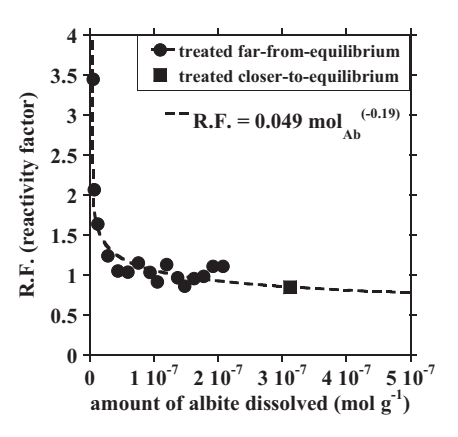


Fig. 9. The change in reactivity factor as a function of the amount of dissolved albite (mol g^{-1}) of the treated albite sample. The squares are the data from the treated far-from-equilibrium albite experiment (see Section 3.3), the dashed curve is fitted to the experimental data set using a power law (Eq. (11)) and the circle is the amount of dissolved albite in the end of the treated closer-to-equilibrium albite experiment. The reactivity factor defined as the ratio of the measured dissolution rate (mol g⁻¹ s⁻¹) divided by the average dissolution rate of the last six measured rates.

extrapolate the rate coefficients from higher temperature regimes. Assuming that the mechanism of Eq. (1) is switched off above $\Delta G_{\rm crit}$, the predicted value of k_1 in Eq. (5) will be 8% higher than k_1 of the present study that is based on the assumption that both mechanisms operate under far-from-equilibrium conditions. This difference is lower than the uncertainty on the measured dissolution rate and therefore is negligible. When the ΔG_r of the solution is under the $\Delta G_{\rm crit}$, under both assumptions the mechanism of Eq. (4) is shut off and therefore not affecting the predicted value of k_2 in Eq. (5).

4.2. The uncertainty on ΔG_{crit}

The only fitted parameter of the model proposed above is the $\Delta G_{\rm crit}$. Using the high temperature data sets (Burch et al., 1993; Alekseyev et al., 1997; Hellmann and Tisserand, 2006), the ΔG_{crit} was estimated to be in the range of -20.9 to -30.6 kJ mol⁻¹. The new experimental data presented in this study is best fitted with $\Delta G_{\rm crit}$ of -36 kJ mol^{-1} . The value of ΔG_{crit} depends on the surface free energy, type of dislocation in the mineral lattice and burgers vector (Lasaga and Blum, 1986; Burch et al., 1993; Lasaga, 1998). These parameters are characteristic properties (intrinsic) of the mineral sample. As there is not enough information about these parameters on the EVJE Norway albite, it is not possible to a priory calculate $\Delta G_{\rm crit}$ for this sample. It is suggested that some of the differences in ΔG_{crit} are due to the different samples used in the current study (EVJE Norway), while previous studies used Amelia Court House. Addition of 10% difference to the mineral surface energy can shift the ΔG_{crit} to the value observed in the present study. Another possible explanation for the different ΔG_{crit} values may be related to differences in extrinsic properties such as temperature and pH. This study describes experiments that were conducted under neutral-acidic pH (\sim 5), while the experiments in the previous works were conducted under basic pH (8.8–9.2). All these possibilities of direct and indirect effects on $\Delta G_{\rm crit}$ will be examined in a future study.

4.3. Extrapolation to 25 °C

Fig. 1d shows a compilation of studies of albite dissolution rate as a function of deviation from equilibrium at 80 °C (Burch et al., 1993), 150 °C (Hellmann and Tisserand, 2006) and 300 °C (Alekseyev et al., 1997) and pH of 8.8, 9.2 and 9, respectively. ΔG_r values were recalculated in the present study using a consistent thermodynamic database (Zhu et al., 2010). In order to present the three data sets on the same plot, the y-axis of the plot is albite dissolution rate normalized to the average far-from-equilibrium (dissolution plateau) rate. The three experimental data sets show sharp change in dissolution rate in the range of -23.02 to -37.68 kJ mol⁻¹. The experimental data at 150 °C have large uncertainties on the measured rates and the data at 300 °C has only one experimental data at the dissolution plateau ΔG_r region. Therefore the rate law (Eq. (5)), which was used to describe the experimental data of all three data sets (solid line named $f(\Delta G_r)$), was fitted only to the data at 80 °C. The agreement between the experimental data at 80, 150 and 300 °C may justify the extrapolation of this rate law to 25 °C.

Based on literature data of albite dissolution rates measured under far-from-equilibrium conditions (Blum and Stillings, 1995) and the above three data sets, the apparent activation energy was calculated to be $-64.9 \pm 3.8 \,\mathrm{kJ} \,\mathrm{mol}^{-1}$. Using this temperature dependence, the rate coefficients of the 80 °C data (which is known with relatively small uncertainty) and the parameters of the fitting of the 80 °C data to the rate law of Eq. (5), the rate coefficients at 25 °C may be predicted to be $k_1 = 5.68 \cdot 10^{-13} + 1.5 \cdot 10^{-13} \,\mathrm{mol} \,\mathrm{m}^{-2} \,\mathrm{s}^{-1}$,

$$k_2 = 5.1 \cdot 10^{-14} + 1.4 \cdot 10^{-14} \text{ mol m}^{-2} \text{ s}^{-1}$$
 (all uncertainties

are 2 s.d.). As the rate is pH independent under approximate neutral pH (Blum and Stillings, 1995), the rate coefficients k_1 and k_2 are expected to be similar in the pH range of 5-9. While the rate coefficients may be predicted using the high temperature data, the value of the Gibbs free energy that is required to form etch pits $(\Delta G_{\rm crit})$ cannot be predicted a priory, and therefore was obtained by fitting the experimental data to be $\Delta G_{\rm crit} =$ --36 kJ mol⁻¹. The solid line in Fig. 10 shows the prediction of the dependence of dissolution rate on deviation from equilibrium at 25 °C and pH \approx 5. The dashed lines represent an uncertainty envelope of 2 standard deviations on the model's predicted rates. As mentioned above, this prediction cannot be confirmed using standard experimental methods. Nevertheless, geochemical models are based on similar unconfirmed extrapolations. The rate data (circles, with error bars of 2 s.d, Fig. 10) are the results of the experiments, which used the treated albite samples. The dissolution plateau data are based on the results of the far-from-equilibrium experiment. The

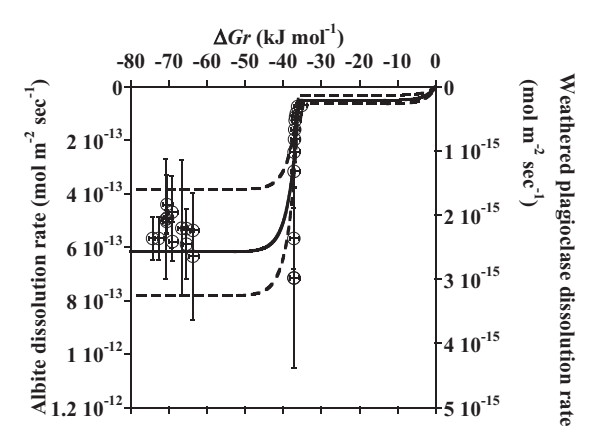


Fig. 10. The change of treated albite dissolution rate at 25 °C as a function of Gibbs free energy. The left y-axis is the measured rates of fresh albite powder. The right y-axis is the predicted rate of weathered plagioclase. The circles are measured dissolution rates without adjustments. Error bars represents two standard deviations. The solid line is a prediction of the rate, which is based on Eq. (5). The rate coefficients are extrapolated from the high temperature data, while $\Delta G_{\rm crit}$ is derived by fitting (see text). The dashed lines represent an envelope of two standard deviation uncertainties on the predicted dissolution rate.

results shown in Fig. 10 describe for the first time albite dissolution rate (or any silicate mineral) as a function of deviation from equilibrium under ambient temperature and circum neutral pH.

4.4. Resolving the gap between laboratory and field rates of weathering

While the new experimental results (Fig. 10) were conducted at temperature, pH and degree of saturation, which are similar to the conditions in nature, the reactivity of the mineral surface, even at the end of the experiment with the treated samples, was significantly larger than that of minerals under natural weathering conditions. White and Brantley (2003) conducted a long term experiment (6 years) in which they examined the change with time in dissolution rate of a weathered plagioclase from the Panola Granite, under laboratory far-from-equilibrium conditions, at 25 °C. They showed that the dissolution rate initially decreased with time and thereafter, within less than a year, was stabilized to be $2.5 \cdot 10^{-15} \,\mathrm{mol}\,\mathrm{m}^{-2}\,\mathrm{s}^{-1}$. As the pH, temperature and the degree of under saturation in White and Brantley (2003) experiment were similar to those in the far-from-equilibrium experiment with the treated albite sample, the difference in dissolution rate can be attributed to difference in the minerals surface reactivity. At the end of their experiment, the weathered plagioclase was about 247 times less reactive than the freshly ground albite after one month of dissolution in the present study. Assuming that the dependence of dissolution rate on deviation from equilibrium does not vary with mineral reactivity, and that the 6-year long experiment of White and Brantley represents the reactivity in the field, this reactivity factor was introduced to the rate law (right y-axis in Fig. 10) by dividing k_1 and k_2 by 247. The modified rate law predicts that the

rate of dissolution of feldspar in the field under the conditions of the Panola Granite ($\Delta G_r = -10.88 \text{ kJ mol}^{-1}$, based on measurements of groundwater chemical composition (White et al., 2001)) is $2.03 \cdot 10^{-16}$ mol m⁻² s⁻¹. This value is in very good agreement with the observed field rate (White et al., 2001) of $2.5 \cdot 10^{-16} \,\text{mol m}^{-2} \,\text{s}^{-1}$, confirming the suggestion of White and Brantley (for further details see Fig. 11 at White and Brantley (2003)). It is important to note that the degree of saturation in the field is closerto-equilibrium than that during the experiments, and the agreement is achieved by using a rate law that was confirmed in the present study at 25 °C further from equilibrium, and is extrapolated to field condition. The agreement between the confirmed rate law and the field data indicates that the extensive debate on the gap between dissolution rates determined using laboratory experiments and those using field observation reflects the inability to measure the dissolution rates under typical field conditions, using standard laboratory experiments (Ganor et al., 2007). The novel method used in the present study resolves this debate and confirms the extrapolation of the rate law from high temperature to ambient conditions.

ACKNOWLEDGEMENTS

This study was supported by The Israel Science Foundation (Grant #297/13) and the Israeli Ministry of Energy and Water Resources (Grant 212-17-012). C. Gruber is grateful for the support by the Yossi Levy Fellowship. We wish to express our gratitude to A. Cohen, A. Reiss and A. Reich for technical assistance. Dina Shtiber and Dr. Olga Yoffe from the Geological Survey of Israel for the chemical analyses of the albite sample. C. Zhu acknowledges NSF Grants EAR-1225733 and the Faculty Research Support Program from Indiana University. Although the work was partly sponsored by an agency of the United States Government, the views and opinions of authors expressed herein do not necessarily state or reflect those of the United States Government or any agency thereof.

REFERENCES

- Alekseyev V. A., Medvedeva L. S., Prisyagina N. I., Meshalkin S. S. and Balabin A. I. (1997) Change in the dissolution rates of alkali feldspars as a result of secondary mineral precipitation and approach to. *Geochim. Cosmochim. Acta* 61, 1125–1142.
- Anbeek C. (1993) The effect of natural weathering on dissolution rates. *Geochim. Cosmochim. Acta* **57**, 4963–4975.
- Arvidson R. S. and Luttge A. (2010) Mineral dissolution kinetics as a function of distance from equilibrium – new experimental results. *Chem. Geol.* 269, 79–88.
- Barrante J. R. (1974) Applied Mathematics for Physical Chemistry. Prentice-Hall Inc., New Jersey.
- Beig M. S. and Luttge A. (2006) Albite dissolution kinetics as a function of distance from equilibrium: implications for natural feldspar weathering. *Geochim. Cosmochim. Acta* 70, 1402–1420.
- Berner R. A. (1992) Weathering, plants and the long term carbon cycle. *Geochim. Cosmochim. Acta* **56**, 3225–3231.
- Bizzarro M., Paton C., Larsen K., Schiller M., Trinquier A. and Ulfbeck D. (2011) High-precision Mg-isotope measurements of terrestrial and extraterrestrial material by HR-MC-ICPMS-implications for the relative and absolute Mg-isotope

- composition of the bulk silicate Earth. *J. Anal. At. Spectrom.* **26.** 565–577.
- Blum A. and Stillings L. L. (1995) Feldspar dissolution kinetics. In Chemical Weathering Rates of Silicate Minerals (eds. A. F. White and S. L. Brantley). Mineralogical Society of America, Washington.
- Brunauer S., Emmett P. H. and Teller E. (1938) Adsorption of gases in multimolecular layers. *J. Am. Chem. Soc.* **60**, 309–319.
- Burch T. E., Nagy K. L. and Lasaga A. C. (1993) Free energy dependence of albite dissolution kinetics at 80 °C, pH 8.8. Chem. Geol. 105, 137–162.
- Casey W. H., Westrich H. R., Massis T., Banfield J. F. and Arnold G. W. (1989) The surface of labradorite feldspar after acid hydrolysis. *Chem. Geol.* 78, 205–218.
- Casey W. H., Banfield J. F., Westrich H. R. and McLaughlin L. (1993) What do dissolution experiments tell us about natural weathering? *Chem. Geol.* **105**, 1–15.
- Chen Y. and Brantley S. L. (1997) Temperature- and pH-dependence of albite dissolution rate at acid pH. *Chem. Geol.* 135, 275–290.
- De La Rocha C. L., Brzezinski M. A. and DeNiro M. J. (2000) A first look at the distribution of the stable isotopes of silicon in natural waters. *Geochim. Cosmochim. Acta* **64**, 2467–2477.
- Dougan W. K. and Wilson A. L. (1974) The absorptiometric determination of aluminum in water. A comparison of some chromogenic reagents and the development of an improved method. *Analyst* **99**, 413–430.
- Douthitt C. B. (1982) The geochemistry of the stable isotopes of silicon. *Geochim. Cosmochim. Acta* 46, 1449–1458.
- Drever J. I. (2003) Surface and ground water, weathering, and soils. In *Treatise on Geochemistry* (eds. H. D. Holland and K. K. Turekian). Elsevier Science, Oxford.
- Drever J. I. and Clow D. W. (1995) Weathering rates in catchments. In *Chemical Weathering Rates of Silicate Minerals* (eds. A. F. White and S. L. Brantley). Mineralogical Society of America, Washington.
- Federer C. A., Hornbeck J., Tritton L., Martin C. W., Pierce R. and Smith C. T. (1989) Long-term depletion of calcium and other nutrients in eastern US forests. *Environ. Manage.* 13, 593–601.
- Fu Q., Lu P., Konishi H., Dilmore R., Xu H., Seyfried, Jr., W. E. and Zhu C. (2009) Coupled alkali-feldspar dissolution and secondary mineral precipitation in batch systems: 1. New experiments at 200 °C and 300°bars. Chem. Geol. 258, 125–135.
- Ganor J., Lu P., Zheng Z. and Zhu C. (2007) Bridging the gap between laboratory measurements and field estimations of silicate weathering using simple calculations. *Environ. Geol.* **53**, 599–610.
- Georg R. B., Reynolds B. C., Frank M. and Halliday A. N. (2006a) Mechanisms controlling the silicon isotopic compositions of river waters. *Earth Planet. Sci. Lett.* 249, 290–306.
- Georg R. B., Reynolds B. C., Frank M. and Halliday A. N. (2006b) New sample preparation techniques for the determination of Si isotopic compositions using MC-ICPMS. *Chem. Geol.* 235, 95– 104.
- Georg R. B., Reynolds B. C., West A. J., Burton K. W. and Halliday A. N. (2007) Silicon isotope variations accompanying basalt weathering in Iceland. *Earth Planet. Sci. Lett.* 261, 476– 490.
- Georg R. B., Zhu C., Reynolds B. C. and Halliday A. N. (2009) Stable silicon isotopes of groundwater, feldspars, and clay coatings in the Navajo Sandstone aquifer, Black Mesa, Arizona, USA. Geochim. Cosmochim. Acta 73, 2229–2241.
- Gruber C., Harpaz L., Zhu C., Bullen T. D. and Ganor J. (2013) A new approach for measuring dissolution rates of silicate

- minerals by using silicon isotopes. *Geochim. Cosmochim. Acta* **104.** 261–280.
- Halicz L., Yang L., Teplyakov N., Burg A., Sturgeon R. and Kolodny Y. (2008) High precision determination of chromium isotope ratios in geological samples by MC-ICP-MS. *J. Anal.* At. Spectrom. 23, 1622–1627.
- Helgeson H. C., Murphy W. M. and Aagaard P. (1984) Thermodynamic and kinetic constraints on reaction rates among minerals and aqueous solutions. II. Rate constants, effective surface area, and the hydrolysis of feldspar. *Geochim. Cosmochim. Acta* 48, 2405–2432.
- Hellmann R. and Tisserand D. (2006) Dissolution kinetics as a function of the Gibbs free energy of reaction: an experimental study based on albite feldspar. *Geochim. Cosmochim. Acta* **70**, 364–383.
- Holdren G. R. and Berner R. (1979) Mechanism of feldspar weathering. I. Experimental studies. *Geochim. Cosmochim. Acta* 43, 1161–1171.
- Huntington T. G., Hooper R. P., Johnson C. E., Aulenbach B. T., Cappellato R. and Blum A. E. (2000) Calcium depletion in forest ecosystems of southeastern United States. Soil Sci. Soc. Am. J. 64, 1845–1858.
- Knauss K. G. and Wolery T. J. (1986) Dependence of albite dissolution kinetics on pH and time at 25 °C and 70 °C. *Geochim. Cosmochim. Acta* **50**, 2481–2497.
- Koroleff F. (1976) Determination of silicon. In Methods of Seawater Analysis (ed. K. Grasshoff). Verlag Chemie, Weinheim.
- Lasaga A. C. (1990) Atomic treatment of mineral-water surface reactions. In *Mineral-Water Interface Geochemistry* (eds. M. F. Hochella and A. F. White). Mineralogical Society of America, Washington.
- Lasaga A. C. (1995) Fundamental approaches in describing mineral dissolution and precipitation rate. In *Chemical Weath*ering Rates of Silicate Minerals (eds. A. F. White and S. L. Brantley). Mineralogical Society of America, Washington.
- Lasaga A. C. (1998) Kinetic Theory in the Earth Sciences. Princeton University Press, Princeton, NJ.
- Lasaga A. C. and Blum A. E. (1986) Surface chemistry, etch pits and mineral-water reactions. *Geochim. Cosmochim. Acta* 50, 2363–2379.
- Lasaga A. C. and Luttge A. (2001) Variation of Crystal Dissolution Rate Based on a Dissolution Stepwave Model.
- Lasaga A. C., Soler J. M., Ganor J., Burch T. E. and Nagy K. L. (1994) Chemical weathering rate laws and global geochemical cycles. *Geochim. Cosmochim. Acta* 58, 2361–2386.
- Likens G. E., Driscoll C. T., Buso D. C., Siccama T. G., Johnson C. E., Lovett G. M., Fahey T. J., Reiners W. A., Ryan D. F., Martin C. W. and Bailey S. W. (1998) The biogeochemistry of calcium at Hubbard Brook. *Biogeochemistry* 41, 89–173.
- Luttge A. (2006) Crystal dissolution kinetics and Gibbs free energy. J. Electron Spectrosc. Relat. Phenom. 150, 248–259.
- Malinovsky D., Stenberg A., Rodushkin I., Andren H., Ingri J., Ohlander B. and Baxter D. C. (2003) Performance of high resolution MC-ICP-MS for Fe isotope ratio measurements in sedimentary geological materials. J. Anal. At. Spectrom. 18, 687–695.
- Moore J., Lichtner P. C., White A. F. and Brantley S. L. (2012) Using a reactive transport model to elucidate differences between laboratory and field dissolution rates in regolith. *Geochim. Cosmochim. Acta* **93**, 235–261.
- Morad S., Al-Ramadan K., Ketzer J. M. and De Ros L. F. (2010) The impact of diagenesis on the heterogeneity of sandstone reservoirs: a review of the role of depositional facies and sequence stratigraphy. AAPG Bull. 94, 1267–1309.

- Opfergelt S., Georg R. B., Burton K. W., Guicharnaud R., Siebert C., Gislason S. R. and Halliday A. N. (2011) Silicon isotopes in allophane as a proxy for mineral formation in volcanic soils. *Appl. Geochem.* **26**(Supplement), S115–S118.
- Opfergelt S., Georg R. B., Delvaux B., Cabidoche Y. M., Burton K. W. and Halliday A. N. (2012) Silicon isotopes and the tracing of desilication in volcanic soil weathering sequences, Guadeloupe. *Chem. Geol.* 326–327, 113–122.
- Oreskes N., Shrader-Frechette K. and Belitz K. (1994) Verification, validation, and confirmation of numerical models in the Earth sciences. *Science* **263**, 641–646.
- Parkhurst D. L. and Appelo C. A. J. (1999) PHREEQC 2.15 A computer program for speciation, batch-reaction, one-dimensional transport and inverse geochemical calculation. Water-Resources Investigation Report 99-4259. U.S. Geological Survey.
- Reeves D. and Rothman D. H. (2013) Age dependence of mineral dissolution and precipitation rates. *Global Biogeochem. Cycles* 27, 906–919.
- Rimstidt J. D. and Barnes H. L. (1980) The kinetics of silica-water reactions. Geochim. Cosmochim. Acta 50, 2509–2516.
- Schnoor J. L. (1990) Kinetics of chemical weathering: a comparison of laboratory and field weathering rates. In *Aquatic Chemical Kinetics: Reaction Rates of Processes in Natural Waters* (ed. W. Stumm). J. Wiley & Sons.
- Spycher N. F., Sonnenthal E. L. and Apps J. A. (2003) Fluid flow and reactive transport around potential nuclear waste emplacement tunnels at Yucca Mountain, Nevada. *J. Contam. Hydrol.* 62–63, 653–673.
- Stumm W. (1992) Chemistry of the Solid-Water Interface. Processes at the Mineral-Water and Particle-Water Interface in Natural Systems. John Wiley & Sons Inc., New York.
- van Grinsven H. J. M. and van Riemsdijk W. H. (1992) Evaluation of batch and column techniques to measure weathering rates in soils. *Geoderma* **52**, 41–57.
- Velbel M. A. (1993) Constancy of silicate-mineral weathering-rate ratios between natural and experimental weathering: implications for hydrologic control of differences in absolute rates. *Chem. Geol.* 105, 89–99.
- White A. F. and Brantley S. L. (1995) Chemical weathering rates of silicate minerals. In *Reviews in Mineralogy* (ed. P. H. Ribbe). Mineralogical Society of America, Washington.
- White A. F. and Brantley S. L. (2003) The effect of time on the weathering of silicate minerals: why do weathering rates differ in the laboratory and field? *Chem. Geol.* **202**, 479–506.
- White A. F., Blum A. E., Schulz M. S., Bullen T. D., Harden J. W. and Peterson M. L. (1996) Chemical weathering rates of a soil chronosequence on granitic alluvium: I. Quantification of mineralogical and surface area changes and calculation of primary silicate reaction rates. *Geochim. Cosmochim. Acta* 60, 2533–2550.
- White A. F., Bullen T. D., Schulz M. S., Blum A. E., Huntington T. G. and Peters N. E. (2001) Differential rates of feldspar weathering in granitic regoliths. *Geochim. Cosmochim. Acta* 65, 847–869.
- White C. M., Strazisar B. R., Granite E. J., Hoffman J. S. and Pennline H. W. (2003) Separation and capture of CO₂ from large stationary sources and sequestration in geological formations—coalbeds and deep saline aquifers. *J. Air Waste Manag. Assoc.* **53**, 645–715.
- White A. F., Schulz M. S., Vivit D. V., Blum A. E., Stonestrom D. A. and Harden J. W. (2005) Chemical weathering rates of a soil chronosequence on granitic alluvium: III. Hydrochemical evolution and contemporary solute fluxes and rates. *Geochim. Cosmochim. Acta* 69, 1975–1996.

- White A. F., Schulz M. S., Vivit D. V., Blum A. E., Stonestrom D. A. and Anderson S. P. (2008) Chemical weathering of a marine terrace chronosequence, Santa Cruz, California I: interpreting rates and controls based on soil concentration—depth profiles. *Geochim. Cosmochim. Acta* 72, 36–68.
- Zhu C. (2005) In situ feldspar dissolution rates in an aquifer. Geochim. Cosmochim. Acta 69, 1435–1453.
- Zhu C. and Anderson G. M. (2002) *Environmental Applications of Geochemical Modeling*. Cambridge University Press, London.
- Zhu C., Blum A. and Veblen D. (2004) Feldspar dissolution rates and clay precipitation in the Navajo aquifer at Black Mesa, Arizona, USA. In: 11th International Symposium on Water-Rock Interaction WRI-11 (eds. R. B. Wanty and R. R. Seal). Balkema, Saratoga Springs, NY, USA.
- Zhu C., Lu P., Zheng Z. and Ganor J. (2010) Coupled alkali feldspar dissolution and secondary mineral precipitation in batch systems: 4. Numerical modeling of kinetic reaction paths. *Geochim. Cosmochim. Acta* **74**, 3963–3983.
- Ziegler K., Chadwick O. A., Brzezinski M. A. and Kelly E. F. (2005a) Natural variations of δ^{30} Si ratios during progressive basalt weathering, Hawaiian Islands. *Geochim. Cosmochim. Acta* **69**, 4597–4610.
- Ziegler K., Chadwick O. A., White A. F. and Brzezinski M. A. (2005b) Δ³⁰Si systematics in a granitic saprolite, Puerto Rico. Geology 33, 817–820.

Associate editor: Fang-zhen Teng